Fuel Efficient Connected Cruise Control for Heavy-Duty Trucks in Real Traffic

Chaozhe R. He, Jin I. Ge, and Gábor Orosz

***Abstract*— In this paper, we present a systematic approach for fuel-economy optimization of a connected automated truck that utilizes motion information from multiple vehicles ahead via vehicle-to-vehicle (V2V) communication. Position and velocity data collected from a chain of human-driven vehicles are utilized to design a connected cruise controller that smoothly responds to traffic perturbations while maximizing energy efficiency. The proposed design is evaluated using a high-fidelity truck model and the robustness of the design is validated on real traffic data sets. It is shown that optimally utilizing V2V connectivity leads to around 10% fuel economy improvements compared to the best nonconnected design.**

***Index Terms*— Connected automated vehicle (CAV), data-based apporach, fuel economy.**

I. Introduction

HEAVY-DUTY vehicles account for a large percentage of fuel consumption in road transportation systems [1]. In order to improve their fuel economy, one may use geolocation information to design optimal speed profiles [2]–[4]. Without traffic perturbations, such optimal speed profiles can lead to over 10% reduction in fuel consumption. However, this benefit may not be attainable in real traffic when a truck has to respond to the speed variations of human-driven vehicles ahead. Although an automated truck using on-board sensors may respond to such scenarios better than a human driver, the fuel-economy improvement may still be limited because on-board sensors can only obtain information within their lines of sight [5].

To further improve fuel economy in real traffic, one answer is to monitor the motion of multiple vehicles ahead and utilize beyond-line-of-sight information through vehicle-to-vehicle (V2V) communication. Some researchers have designed centralized and cooperative controllers for platoons of automated trucks [6], [7], so that each participating truck can enjoy significant fuel improvement [8], [9]. However, it can be tricky to organize such cooperative platoons, before automated trucks become widespread [10]. Therefore, noncooperative schemes have been proposed to predict the preceding vehicle's motion and optimize fuel economy in a receding horizon manner [11]–[14]. Yet such methods often have heavy computational load [15], and their performance in real traffic is unclear when the prediction accuracy may not be guaranteed. While stochastic approaches and off-line methods can be used to alleviate such limitations [16], examples from other research areas indicate that simpler design schemes may be more applicable and even perform better in real application scenarios [17].

Therefore, we directly included V2V information from multiple vehicles ahead in the feedback structure and proposed the concept of connected cruise control [18]. A vehicle driven by such a connected cruise controller is referred to as a connected automated vehicle (CAV). Although, in practice, a CAV may have higher level of autonomy, here, we only require longitudinal automation. While a small percentage of CAVs on the road can already improve traffic safety and efficiency [19], [20], the CAV itself can also achieve better fuel economy theoretically [15], [21], [22]. Yet the question remains whether connected cruise control can indeed save fuel in real traffic. To answer this question, here, we present a data-driven design for connected cruise control that improves fuel economy by minimizing the overall energy consumption. Compared to our preliminary works reported in [22], the main contributions of this paper are as follows.

1) We propose a design method that fully exploits the traffic data available from preceding vehicles without assuming car-following models for preceding vehicles.
2) We take into account all relevant nonlinearities in the control design.
3) We carry out a robustness study to evaluate the performance against different traffic scenarios.
4) We compare the performance with the widely researched receding-horizon controllers.

The remainder of this paper is organized as follows. In Section II, as a motivation for the proposed design, we use real traffic data to analyze the influence of traffic perturbations on a truck's fuel consumption using a high-fidelity model. We demonstrate that the majority of fuel consumption in traffic is due to the energy consumption related to speed fluctuations. In Section III, we present a connected cruise control design that utilizes motion information of multiple vehicles ahead to minimize energy consumptions in traffic. The proposed design is evaluated in Section IV using real traffic data sets, and the results are also compared to those obtained using receding-horizon controllers. Finally, the conclusions are given in Section V.

II. Motivation: Saving Fuel in Traffic

In this section, we demonstrate the impact of traffic perturbations on a truck's fuel consumption using real traffic data.

Manuscript received February 1, 2019; revised June 8, 2019; accepted June 24, 2019. Date of publication July 26, 2019; date of current version October 9, 2020. Manuscript received in final form June 25, 2019. This work was supported by the University of Michigan Mobility Transformation Center. Recommended by Associate Editor N. Quijano. *(Corresponding author: Chaozhe R. He.)*

C. R. He and G. Orosz are with the Department of Mechanical Engineering, University of Michigan, Ann Arbor, MI 48109 USA (e-mail: hchaozhe@umich.edu; orosz@umich.edu).

J. I. Ge is with the Department of Computing and Mathematical Sciences, California Institute of Technology, Pasadena, CA 91125 USA (e-mail: jge@caltech.edu).

This article has supplementary downloadable material available at http://ieeexplore.ieee.org, provided by the author.

Color versions of one or more of the figures in this article are available online at http://ieeexplore.ieee.org.

Digital Object Identifier 10.1109/TCST.2019.2925583

1063-6536 © 2019 IEEE. Personal use is permitted, but republication/redistribution requires IEEE permission.
See https://www.ieee.org/publications/rights/index.html for more information.

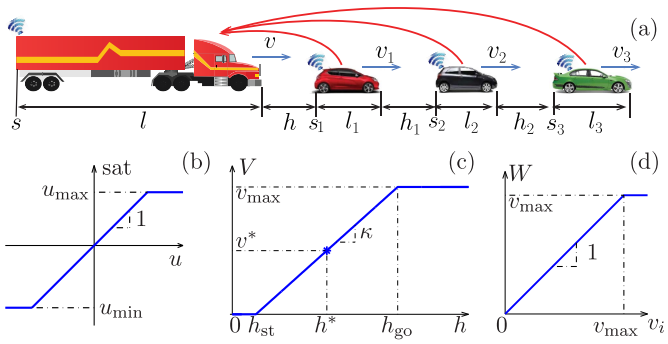


Fig. 1. (a) A truck driving behind three human-driven vehicles on a single-lane road. (b) Saturation function in (1). (c) Range policy function (6). (d) Saturation function (7).

We show that, while such impacts can be reduced by tuning the longitudinal controller through high-fidelity simulations, a systematic optimization method is needed for more robust designs.

We consider a driving scenario where a truck drives behind several human-driven vehicles on a segment of single lane with no elevation [see Fig. 1(a)] where the arrows represent the potential information flow to the truck from preceding vehicles. The longitudinal motion of the truck can be described by

$$\begin{aligned} \dot{s}(t) &= v(t), \\ \dot{v}(t) &= -f\big(v(t)\big) + \mathrm{sat}\Big(\tilde{f}\big(v(t-\zeta)\big) + a_{\mathrm{d}}(t-\zeta)\Big) \end{aligned} \tag{1}$$

where the dot denotes differentiation with respect to time t, s denotes the position of the rear bumper of the truck, v denotes its velocity, and ζ is the actuator delay that can also be approximated by a first order lag [14], [18].

The physical effects such as air resistance and rolling resistance can be described by

$$f(v) = \frac{1}{m_{\mathrm{eff}}}(\gamma m g + k_0 v^2), \tag{2}$$

where g is the gravitational constant, γ is the rolling resistance coefficient, and k_0 is the air drag constant. The effective mass $m_{\mathrm{eff}} = m + I/R^2$ includes the mass of the vehicle m, the moment of inertia I of the rotating elements, and the wheel radius R [4]. To compensate for these physical effects, the term $\tilde{f}$ is often added through a lower level controller. Finally, a_{d} denotes the higher level acceleration command, which is limited between $u_{\min}$ and $u_{\max}$ by the saturation function

$$\mathrm{sat}(u) = \begin{cases} u_{\min}, & \text{if } u \le u_{\min} \\ u, & \text{if } u_{\min} < u < u_{\max} \\ u_{\max}, & \text{if } u \ge u_{\max} \end{cases} \tag{3}$$

based on the engine and braking power limit [see Fig. 1(b)]. Table I includes the parameter values used in this paper.

If the truck is driven by a human driver or adaptive cruise controller, the higher level controller in (1) can be given as

$$\begin{aligned} a_{\mathrm{d}}(t) = \alpha\Big(V\big(h(t-\xi_1)\big) - v(t-\xi_1)\Big) \\ + \beta_1\Big(W\big(v_1(t-\xi_1)\big) - v(t-\xi_1)\Big). \end{aligned} \tag{4}$$

TABLE I

CONSTANT PARAMETERS USED IN THE CONNECTED CRUISE CONTROL DESIGN

α	0.4 [1/s]	κ	0.6 [1/s]
$u_{\max}$	1 [m/s^2]	$u_{\min}$	-4 [m/s^2]
σ	0.7 [1/s]	$v_{\max}$	30 [m/s]
h_{st}	5[m]		

In this case, only information from vehicle 1 is used. Here, α and β_1 are the feedback gains, while the headway

$$h = s_1 - s - l \tag{5}$$

is the distance gap between the truck and its preceding vehicle, where l denotes the length of the truck [see Fig. 1(a)]. Finally, ξ_1 represents the sensory delay of position and speed information from vehicle 1.

The range policy function

$$V(h) = \begin{cases} 0, & \text{if } h \le h_{\mathrm{st}} \\ \kappa(h - h_{\mathrm{st}}), & \text{if } h_{\mathrm{st}} < h < h_{\mathrm{go}} \\ v_{\max}, & \text{if } h \ge h_{\mathrm{go}} \end{cases} \tag{6}$$

describes the desired velocity of the truck as a function of its headway [see Fig. 1(c)]. For a small headway ($h < h_{\mathrm{st}}$), the truck intends to stop, and for a large headway ($h > h_{\mathrm{go}}$), it intends to travel with the speed limit $v_{\max}$; between h_{st} and h_{go}, the desired velocity increases linearly with the gradient $\kappa = v_{\max}/(h_{\mathrm{go}} - h_{\mathrm{st}})$. Finally, the saturation function

$$W(v_1) = \begin{cases} v_1, & \text{if } v_1 \le v_{\max} \\ v_{\max}, & \text{if } v_1 > v_{\max} \end{cases} \tag{7}$$

shown in Fig. 1(d) is included to stay below the speed limit when the preceding vehicle is speeding [see Table I for the parameter values used in this paper].

In order to relate the motion obtained by (1) and (2) to the fuel consumption, we define the cumulative energy consumption for the truck per unit mass

$$w(t) = \int_{t_0}^{t} v(\tilde{t})\, g\Big(\dot{v}(\tilde{t}) + f\big(v(\tilde{t})\big)\Big)\, \mathrm{d}\tilde{t} \tag{8}$$

where $t \in [t_0, t_{\mathrm{f}}]$ and $g(x) = \max(0, x)$. For vehicles with internal combustion engines, fuel consumption typically increases with the energy consumption $w(t)$. However, as $w(t)$ is defined by the vehicle's motion, it can also be used to evaluate the energy consumption of electric or hybrid vehicles due to speed variations using an appropriate g function. The effectiveness of using (8) for designing fuel-efficient control algorithms will be demonstrated later in this section.

To calculate the fuel consumption with higher accuracy, we also build a high-fidelity model in TruckSim based on a 2012 Navistar Prostar truck including its accurate fuel map [22]. While fuel maps can be obtained for the purpose of validation, a controller design that does not require fine tuning based on accurate fuel maps may be more robust and easier to implement.

In order to describe the traffic perturbations, we track the motion of three consecutive human-driven vehicles in traffic.

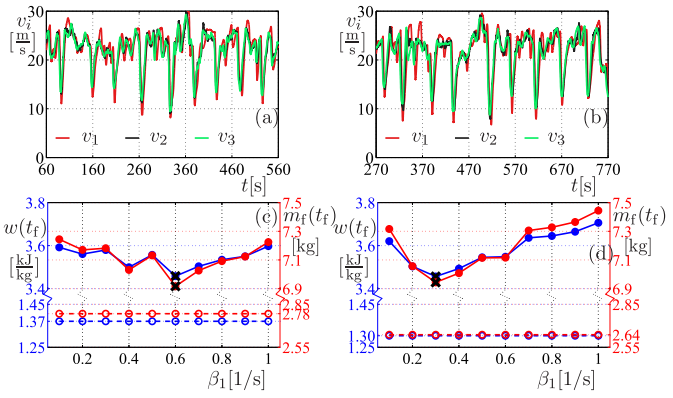


Fig. 2. (a) and (b) Speed profiles of preceding human-driven vehicles, where the red, black, and green curves represent v_1, v_2, and v_3, respectively. (c) and (d) Total energy consumption (8) at the end of each run for different values of the control gain β_1 is shown as blue dots. The total mass of fuel m_f consumed by the truck for the same parameters is shown as red dots. Black crosses denote the minima. For comparison, the values corresponding to constant speed are also plotted as blue and red circles connected by dashed lines.

Two sets of the recorded speed data are plotted in Fig. 2(a) and (b), where the green, black, and red curves correspond to the speed of vehicle 3, vehicle 2, and vehicle 1, respectively [see Fig. 1(a)]. In both cases, while the human-driven vehicles travel with average speed of $v^* \approx 22$ [m/s], their speed data exhibit large variations that are often observed in dense traffic. Comparing the Fourier spectra of these speed profiles can reveal the similarity between the different profiles as will be discussed in Section IV.

Using the high-fidelity simulation platform, we can simulate the truck responding to speed perturbations shown in Fig. 2(a) and (b) and calculate its energy consumption (8) as well as the fuel consumption for different values of the feedback parameters in the controller (4). In Fig. 2(c) and (d), we plot the total energy consumption (blue dots) and the total fuel consumption (red dots) of the truck during each simulation for $\beta_1 \in \{0.1, \ldots, 1.0\}$ [1/s]. The parameters $\kappa = 0.6$ [1/s] and $\alpha = 0.4$ [1/s] are selected based on previous experiments [20], since these gave a good balance between car-following performance and safety [see Table I]. In Fig. 2(c), the truck consumes the least amount of energy when $\beta_1 = 0.6$ [1/s] and it also consumes the least amount of fuel for the same value. This indicates that one may minimize fuel consumption through minimizing energy consumption while tuning the feedback gains in the higher level controller (4).

If there were no speed perturbations, i.e., the preceding vehicles had a constant speed, the truck could also maintain the same constant speed. Then, it would consume the total energy $w(t_f) = 1.37$ [kJ/kg] and the total fuel $m_f(t_f) = 2.78$ [kg] [see the blue and red circles along the dashed lines in Fig. 2(c)]. While constant-speed driving comprises less than half of the total fuel/energy consumption, such motion can rarely be achieved in real traffic. Nevertheless, the truck may reduce its energy consumption toward the constant-speed level, if it is able to minimize its speed variation despite the traffic perturbations. In particular, such smooth speed profiles can be achieved using connected cruise control, where V2V signals from vehicles ahead serve as a "preview" of incoming traffic situations.

Since the energy consumption (8) well approximates the fuel consumption in the high-fidelity simulation, one may decide to use this quantity (rather than the fuel map) in order to achieve the best fuel economy. Note that, while the high-fidelity simulation platform can readily provide optimal controller gains, given specific speed profiles, it can be costly in computation, and the optimal design may be sensitive to the speed profiles. For example, based on Fig. 2(c), one may be tempted to set $\beta_1 = 0.6$ [1/s] for the truck driving in such slow-and-go traffic. However, in Fig. 2(d), for similar speed profiles, the energy and fuel minima are reached at $\beta_1 = 0.3$ [1/s].

In order to eliminate such sensitivity (that is partially caused by the nonlinearities in the powertrain dynamics), one may use the simplified model (1), (2) and the energy consumption (8) to optimize the higher level controllers (4) through a simulation-based approach. Let alone the costly computation of this approach, similar sensitivity may still be observed due to the nonlinearities in (1), (6), and (7). In order to extract the essential dynamics, in the next section, we linearize the models (1) and (2), and build up an analytical approach to approximate the energy consumption (8). This will result in a computationally efficient method that is robust against changes in the speed profiles and allows us to utilize V2V signals optimally in order to improve the fuel economy of the truck. The high-fidelity simulation platform will still be used for evaluation in Section IV.

III. Data-Driven Connected Cruise Control Design

In this section, we consider a connected cruise controller for the truck which includes direct feedback on speed signals from n human-driven vehicles ahead [see red arrows in Fig. 1(a)]. Note that each human-driven vehicle responds to the motion of the vehicle immediately ahead.

We propose the connected cruise controller

$$a_d(t) = \alpha\Big(V\big(h(t-\xi_1)\big) - v(t-\xi_1)\Big) + \sum_{i=1}^{n} \beta_i \Big(W\big(v_i(t-\xi_i)\big) - v(t-\xi_i)\Big) \tag{9}$$

for the connected automated truck (cf., (4)) and recall that h is the headway defined in (5). We remark that such design is based on our previous theoretical and experimental studies [20], [23], [24].

The speed signals from vehicles farther ahead can be viewed as "preview information" about speed variations propagating toward the connected automated truck. By including v_i, $i = 2, \ldots, n$, in the feedback structure, the connected cruise controller (9) gains "phase lead" against variations in the speed v_1 of its immediate predecessor. In this way, (9) enjoys the advantages of many cooperative adaptive cruise control designs [10] without requiring the support of an automated vehicle fleet. While headway, speed, and acceleration from multiple preceding vehicles can be used

in connected cruise control [24], [25], here, we only use V2V speed signals for simplicity.

Our design goal is to find the optimal gains in the controller (9) such that the response generated by (1), (2) minimizes the energy consumption (8). First, we linearize (1), (2), and (9) about the average speed. The transient response of the linearized model is analyzed in order to find gain combinations that ensure stability. The steady-state response of the linearized model to traffic perturbations is generated using the velocity data of preceding vehicles. We use this response to optimize the gains in the connected cruise controller (9) in order to achieve the best energy efficiency in a computationally efficient way.

The equilibrium is given by the average speed

$$v(t) \equiv v_i(t) \equiv v^* \tag{10}$$

for $i = 1, \ldots, n$ and

$$h(t) \equiv h^*, \quad v^* = V(h^*) \tag{11}$$

see (6) and Fig. 1(c).

We define $\tilde{s}$, $\tilde{s}_1$, $\tilde{v}_i$, $i = 1, \ldots, n$ as the perturbations about the equilibrium positions and velocities and assume that the influence of the physical effects $f(v)$ can be negated by $\tilde{f}(v)$. Then linearizing the dynamics [see (1) and (9)] of the connected automated truck about (10), we obtain

$$\begin{aligned}\dot{\tilde{s}}(t) &= \tilde{v}\\ \dot{\tilde{v}}(t) &= \alpha\Big(\kappa\big(\tilde{h}(t-\sigma_1)\big) - \tilde{v}(t-\sigma_1)\Big)\\ &\quad + \sum_{i=1}^{n} \beta_i\Big(\tilde{v}_i(t-\sigma_i) - \tilde{v}(t-\sigma_i)\Big)\end{aligned} \tag{12}$$

where $\tilde{h} = \tilde{s}_1 - \tilde{s}$ is the perturbation about the equilibrium headway h^* and $\sigma_i = \xi_i + \zeta$ for $i = 1, \ldots, n$ gives the total delay in the control loop. For simplicity, we consider $\sigma_i = \sigma$ for $i = 1, \ldots, n$, [see Table I].

A. Stability Condition for Maintaining Constant Speed

In order for the connected automated truck to be able to maintain its speed around the equilibrium [e.g., keep the same constant speed as preceding vehicles while having the headway according to (6)], we require the linearized dynamics [see (12)] to be plant stable [18]. This is ensured when all roots of the characteristic equation

$$D(\lambda) = \lambda^2 \mathrm{e}^{\sigma\lambda} + \left(\alpha + \sum_{i=1}^{n} \beta_i\right)\lambda + \alpha\kappa = 0 \tag{13}$$

are located in the left half complex plane. Thus, the design parameters α and β_i need to be selected from the domain enclosed by

$$\alpha = 0, \tag{14}$$

and

$$\begin{aligned}\alpha &= \frac{\Omega^2}{\kappa}\cos(\Omega\sigma),\\ \sum_{i=1}^{n} \beta_i &= \Omega\sin(\Omega\sigma) - \frac{\Omega^2}{\kappa}\cos(\Omega\sigma)\end{aligned} \tag{15}$$

for $\Omega > 0$.

B. Data-Driven Minimization on Energy Consumption

Based on the linearized dynamics (12), the steady-state speed oscillation of the connected automated truck can be written as

$$\tilde{V}(\lambda) = \sum_{i=1}^{n} \Gamma_i(\lambda; \mathbf{p}_n)\tilde{V}_i(\lambda) \tag{16}$$

where $\tilde{V}_i(\lambda)$ is the Laplace transform of the velocity perturbation $\tilde{v}_i(t)$, the vector $\mathbf{p}_n = [\beta_1, \ldots, \beta_n]$ contains the design parameters, and the so-called link transfer function from the ith vehicle to the connected automated truck can be formulated as

$$\begin{aligned}\Gamma_1(\lambda; \mathbf{p}_n) &= \frac{\alpha\kappa + \lambda\beta_1}{\lambda^2\mathrm{e}^{\sigma\lambda} + \left(\alpha + \sum_{k=1}^{n}\beta_k\right)\lambda + \alpha\kappa}\\ \Gamma_i(\lambda; \mathbf{p}_n) &= \frac{\lambda\beta_i}{\lambda^2\mathrm{e}^{\sigma\lambda} + \left(\alpha + \sum_{k=1}^{n}\beta_k\right)\lambda + \alpha\kappa}\end{aligned} \tag{17}$$

for $i = 2, \ldots, n$.

The velocity perturbation of vehicle i can be described using the m leading Fourier components

$$\tilde{v}_i(t) = \sum_{j=1}^{m} \rho_{i,j}\sin(\omega_j t + \phi_{i,j}), \tag{18}$$

where we discretized frequency $\omega_j = j\Delta\omega$, with $\Delta\omega = 2\pi/(t_\mathrm{f} - t_0)$. Moreover, $\rho_{i,j} = \rho_i(\omega_j)$ and $\phi_{i,j} = \phi_i(\omega_j)$ are the amplitude and phase angle of speed oscillations at frequency ω_j for car i.

Based on (16)–(18), the steady-state oscillation of the connected automated truck is given by

$$\tilde{v}(t) = \sum_{j=1}^{m}\sum_{i=1}^{n} \tilde{\rho}_{i,j}(\mathbf{p}_n)\sin(\omega_j t + \tilde{\phi}_{i,j}(\mathbf{p}_n)) \tag{19}$$

where

$$\begin{aligned}\tilde{\rho}_{i,j}(\mathbf{p}_n) &= \rho_{i,j}\Gamma_i(\mathrm{i}\omega_j; \mathbf{p}_n)\\ \tilde{\phi}_{i,j}(\mathbf{p}_n) &= \phi_{i,j} + \angle\,\Gamma_i(\mathrm{i}\omega_j; \mathbf{p}_n).\end{aligned} \tag{20}$$

This can be rewritten as

$$\tilde{v}(t) = \sum_{j=1}^{m} D_j(\mathbf{p}_n)\sin\left(\omega_j t + \theta_j(\mathbf{p}_n)\right) \tag{21}$$

where

$$\begin{aligned}D_j &= \sqrt{\left(\sum\nolimits_{i=1}^{n}\tilde{\rho}_{i,j}\cos\tilde{\phi}_{i,j}\right)^2 + \left(\sum\nolimits_{i=1}^{n}\tilde{\rho}_{i,j}\sin\tilde{\phi}_{i,j}\right)^2}\\ \tan\theta_j &= \left(\sum_{i=1}^{n}\tilde{\rho}_{i,j}\sin\tilde{\phi}_{i,j}\right)\Big/\left(\sum_{i=1}^{n}\tilde{\rho}_{i,j}\cos\tilde{\phi}_{i,j}\right).\end{aligned} \tag{22}$$

Formulae (17), (19), (21), and (22) can be used to construct the steady state response of the connected automated truck to the signals given in (18) and calculate the energy consumption using formula (8). However, this could still be computationally expensive, particularly if the dimension of $\mathbf{p}_n$ is large. To further simplify the computation, we construct

the upper and lower bounds for (8) in [26] as a class-$\mathcal{K}$ function of the cost function

$$J_n(\mathbf{p}_n) = \sum_{j=1}^{m} \omega_j^2 D_j^2(\mathbf{p}_n) \tag{23}$$

see the supplemental material [26].

Minimizing the cost function (23), we may find the optimal parameter $\mathbf{p}_n^*$ within the admissible set $\mathbf{P}$ where $\mathbf{p}_n \in \mathbf{P}$ ensures plant stability [see (14) and (15)]. By computing the level sets of (23), the parameters in $\mathbf{p}_n$ can be related to the energy efficiency of the connected automated truck. Other specifications such as string stability may also be incorporated [21]. We remark that the computational demand of such minimization is very low as the cost function (23) does not require the reconstruction of the steady-state response in the time domain. In Section IV, we will demonstrate that, while being derived after multiple simplifications, this analytical, yet data-driven approach, will allow us to achieve robust performance against changes in traffic scenarios.

IV. Minimizing Energy Consumption of Connected Cruise Control in Traffic

In this section, we obtain the optimal β_i values in (9) using (23) while utilizing real traffic data (see Fig. 2). We also evaluate the corresponding fuel consumption for the connected automated truck using the same high-fidelity simulation platform as before. We first establish the benchmark design where the truck only uses motion information from its immediate predecessor. We then present the energy-optimal connected cruise control design and demonstrate its robustness against differences in speed perturbations. Finally, we compare the performance of the optimal CCC to that of a receding horizon controller.

A. Using Motion Information From One Vehicle Ahead

To establish a benchmark for the controller that exploits information from multiple vehicles ahead, we first consider the case where the truck only uses motion information from vehicle 1, i.e., (9) reduces to (4) and β_1 is the only design parameter. We use the Fourier spectrum of the speed profiles v_1 in the cost function (23) that is shown as a function of β_1 in Fig. 3(a). The blue and red curves correspond to the profiles shown in the left and right columns of Fig. 2 and in both cases the minima are at $\beta_1 = 0.4$ [1/s] as indicated by black crosses. That is, in contrast to the variation of optimal β_1 in Fig. 2(c) and (d), the optimal β_1 in Fig. 3(a) remains the same for the different speed profiles. We refer to the optimal parameter set $[\beta_1, \beta_2, \beta_3] = [0.4, 0, 0]$ [1/s] as the "benchmark design" in the remainder of this paper.

Recall that the cost function (23) was constructed to avoid the direct calculation of the energy consumption (8). However, using the Fourier components (22), one may still reconstruct the steady-state response (21) in the time domain and calculate (8). The corresponding values are shown as a function of β_1 in Fig. 3(b). Again, blue and red curves correspond to the profiles in the left and right columns of Fig. 2. While the minima are slightly different compared to Fig. 3(a), both

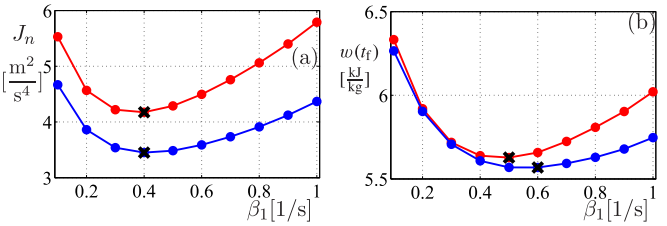


Fig. 3. (a) Value of cost function (23) and (b) energy consumption function (8) for different values of the control gain β_1. The blue and red curves correspond to the speed profiles in the left and the right columns of Fig. 2, respectively. Black crosses denote the minima.

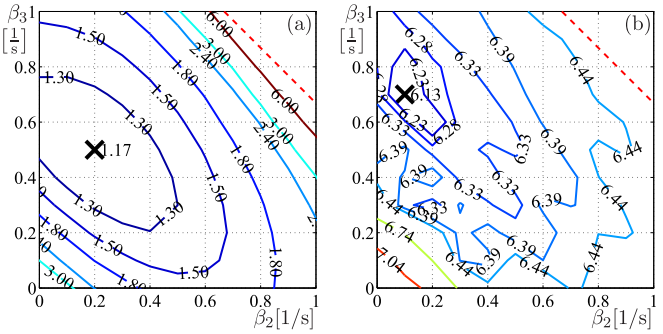


Fig. 4. (a) Level sets of the cost function (23) in the (β_2, β_3)-plane for $\beta_1 = 0.1$ [1/s]. (b) Level sets of the total fuel consumption $m_\mathrm{f}(t_\mathrm{f})$ in the (β_2, β_3)-plane for $\beta_1 = 0.1$ [1/s]. The black crosses denote the minima. The red dashed line corresponds to the stability boundary (15).

panels follow the same trend as β_1 is varied. This demonstrates that eliminating the nonlinearities (powertrain dynamics and saturations) allows us to reveal the key dynamics behind the energy consumption and achieve robust design. We will continue using (23) as the design cost function to acquire optimal gains.

B. Using Motion Information From Multiple Vehicles Ahead

We now utilize motion information from vehicles 1, 2, and 3 in the connected cruise controller (9). We consider the admissible range of β_i based on the linear stability region defined by (15). Considering $\beta_1, \beta_2, \beta_3 \in \{0.1, \ldots, 1.0\}$ [1/s], we compute the cost function (23), and obtain the corresponding fuel consumption $m_\mathrm{f}(t_\mathrm{f})$ using the high-fidelity platform.

Fig. 4(a) shows the level sets of the cost function (23) in the (β_2, β_3)-plane for $\beta_1 = 0.1$ [1/s] when the truck responds to the speed perturbations shown in Fig. 2(a). The red dashed curve corresponds to the stability boundary (15). The global minimum $J_n^* = 1.17$ [$\mathrm{m}^2/\mathrm{s}^4$] is achieved at $\mathbf{p}_n^* = [\beta_1^*, \beta_2^*, \beta_3^*] = [0.1, 0.2, 0.5]$ [1/s], as marked by the black cross in Fig. 4(a). In the remainder of this paper, we refer this as the "energy-optimal CCC design." Note that not only the minimum is significantly smaller than the minima in Fig. 3(a) but most contours in Fig. 4(a) indicate lower cost than in Fig. 3(a). This shows the energy-saving potentials of including speed data from vehicles farther ahead.

In Fig. 4(b) we show the corresponding level sets of the total fuel consumption $m_\mathrm{f}(t_\mathrm{f})$ for $\beta_1 = 0.1$ [1/s] obtained via

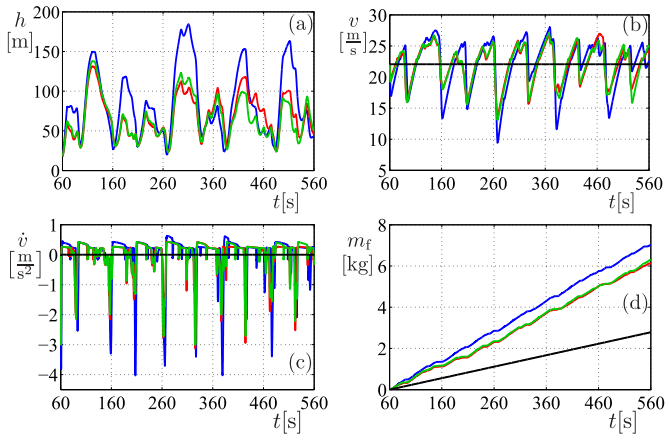


Fig. 5. Time profiles for the connected automated truck. The blue curves correspond to the benchmark design when motion information only from vehicle 1 is used ($[\beta_1, \beta_2, \beta_3] = [0.4, 0.0, 0.0]$ [1/s]). The green curves correspond to the energy-optimal CCC design when motion information from vehicles 1, 2, and 3 are utilized ($[\beta_1, \beta_2, \beta_3] = [0.1, 0.2, 0.5]$ [1/s]). The red curves correspond to the fuel-optimal CCC design when motion information from vehicles 1, 2, 3 are utilized ($[\beta_1, \beta_2, \beta_3] = [0.1, 0.1, 0.7]$ [1/s]). The solid black lines correspond to the constant speed profile without traffic disturbance.

high-fidelity Trucksim simulations. The fuel-optimal parameter combination is at is $[\beta_1, \beta_2, \beta_3] = [0.1, 0.1, 0.7]$ [1/s], as marked by the black cross. In the remainder of this paper, we refer to this as the "fuel-optimal CCC design". This is close to the energy-optimal parameters [black cross in Fig. 4(a)]. Again, most level sets in Fig. 4(b) show less fuel consumption than the minimum of the red curve in Fig. 2(c). This indicates that even with nonlinearities in the longitudinal controller and powertrain dynamics having the traffic speed farther ahead can help to improve fuel economy. Fig. 4 also highlights the similarities between the cost function (23) [derived from (8)], and the actual fuel consumptions given by the high fidelity platform where all relevant nonlinearities are included.

To further demonstrate the benefits of utilizing motion information from vehicles farther ahead, we plot the time profiles corresponding to the benchmark parameters $[\beta_1, \beta_2, \beta_3] = [0.4, 0, 0]$ [1/s] in blue, the energy-optimal CCC parameters $[\beta_1, \beta_2, \beta_3] = [0.1, 0.2, 0.5]$ [1/s] in green, and the fuel-optimal CCC parameters $[\beta_1, \beta_2, \beta_3] = [0.1, 0.1, 0.7]$ [1/s] in red in Fig. 5. We also plot the speed and fuel consumption profiles that correspond to constant speed as solid black lines. Note that the two CCC designs have much smaller headway, speed, and acceleration variations, which contributes to smaller fuel consumption. While the energy-optimal and fuel-optimal parameters generate different trajectories, the difference is quite small.

When looking at the total fuel consumption $m_f(t_f)$ at the end of the simulations in Fig. 5(d), the energy-optimal CCC design (green) consumes about 10.4% less fuel than the benchmark design, while the fuel-optimal CCC design consumes about 12.8% less fuel than the benchmark design. Fig. 5(c) highlights the reason behind this significant improvement: in each cycle of speed perturbation, the energy/fuel-optimal designs accelerate/brake earlier and milder than the benchmark design. With less energy dissipated in braking, the connected automated truck requests less energy from the engine and consumes less fuel.

TABLE II
FUEL CONSUMPTION, CAR-FOLLOWING, AND SAFETY PERFORMANCE FOR THE BENCHMARK, ENERGY-OPTIMAL CCC, AND FUEL-OPTIMAL CCC DESIGNS

design	benchmark	energy-optimal CCC	fuel-optimal CCC
$[\beta_1, \beta_2, \beta_3]$[1/s]	[0.4, 0, 0]	[0.1, 0.2, 0.5]	[0.1, 0.1, 0.7]
$m_f(t_f)$ [kg]	7.03	6.30	6.13
Δh_{avg}[m]	44.1	25.7	17.9
TTC [s]	4.0	5.9	6.1

Aside from the energy/fuel benefits of the CCC designs, we also quantify the car-following performance using the average headway error

$$\Delta h_{\text{avg}} = \frac{1}{t_f - t_0} \int_{t_0}^{t_f} \left| h(t) - h_{\text{st}} - \frac{v(t)}{\kappa} \right| \mathrm{d}t \tag{24}$$

and quantify the safety performance using the minimal time-to-collision

$$\text{TTC} = \min_t \left\{ \frac{h(t)}{v(t) - v_1(t)} \,\middle|\, \forall\, v(t) > v_1(t) \right\}. \tag{25}$$

The total fuel consumption $m_f(t_f)$, the average headway error Δh_{avg}, and the minimal time-to-collision (TTC) are summarized in Table II. Based on this data we can conclude that by introducing motion information from vehicles farther ahead, fuel economy, car-following performance, and safety are improved for the connected automated truck. Moreover, the energy-optimal design acquired using (23) can achieve near optimal fuel performance without carrying out extensive simulations.

C. Robustness of CCC Design

For a connected automated truck responding to the speed profiles shown in Fig. 2(a), we have obtained a benchmark design when information from its immediate predecessor is used, and energy-optimal and fuel-optimal designs when information from three vehicles ahead is used. However, the exact speed profiles used in these designs may not recur in real traffic. Thus, it is critical that, given similar speed profiles, the energy/fuel-optimal gains maintain their benefits over the benchmark design. Here, we evaluate the robustness of the energy-optimal design using six sets of traffic data. For the details of how the data were collected please see [20].

To measure the difference between sets I and J, we propose the metric

$$\text{Dis}(I, J) = \frac{1}{n} \sum_{i=1}^{n} \left(\sum_{j=1}^{m} \left(\tilde{\rho}_{i,j}^{I} - \tilde{\rho}_{i,j}^{J} \right)^2 \right) \tag{26}$$

where n refers to furthest vehicle ahead considered in the design, while m indicates maximum frequency components [cf., (19)].

In Fig. 6(a), the distance between set 1 and the other sets are shown. Fig. 6(b)–(e) shows the improvements of cost function (23), the fuel consumption, the average headway error (24),

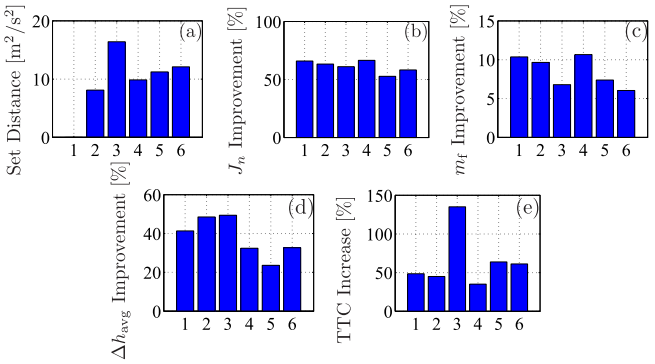


Fig. 6. Performance improvements of the energy-optimal CCC design ($[\beta_1, \beta_2, \beta_3] = [0.1, 0.2, 0.5]$) over the benchmark design ($[\beta_1, \beta_2, \beta_3] = [0.4, 0, 0]$).

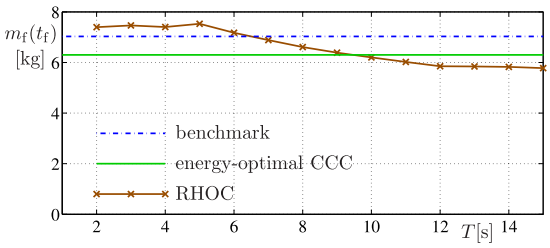


Fig. 7. Total fuel consumption of RHOC design as a function of preview horizon T, compared to the benchmark design (blue dashed-dotted line) and the energy-optimal CCC design (solid green line).

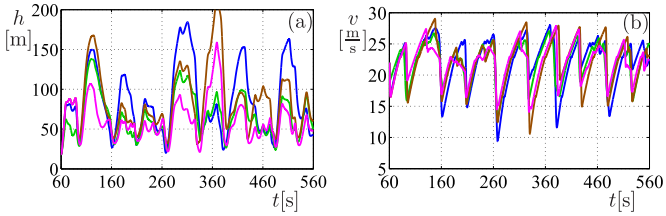


Fig. 8. Time profiles for the connected automated truck. The blue curves corresponds to the benchmark design when motion information only from vehicle 1 is used ($[\beta_1, \beta_2, \beta_3] = [0.4, 0.0, 0.0]$ [1/s]). The green curves corresponds to the energy-optimal CCC design when motion information from vehicles 1, 2, and 3 are utilized ($[\beta_1, \beta_2, \beta_3] = [0.1, 0.2, 0.5]$ [1/s]). The brown curves corresponds to the RHOC design with $T = 5$ s, while the magenta curve corresponds to the RHOC design with $T = 10$ s.

and the minimal time-to-collision (25) of the energy-optimal CCC design ($[\beta_1, \beta_2, \beta_3] = [0.1, 0.2, 0.5]$ [1/s]) compared to the benchmark design ($[\beta_1, \beta_2, \beta_3] = [0.4, 0, 0]$ [1/s]) for the six data sets. It can be seen that the energy-optimal gains continue to produce 6%–12% improvement in energy efficiency/fuel economy, while improvement in car-following performance and safety can also be obtained. These results demonstrate that the proposed design approach can benefit the fuel economy, car-following performance, and safety of the connected automated truck, and such benefits are robust against traffic variations.

We remark that for those sets whose distance from set 1 are larger (such as sets 3, 5, and 6), the improvements are less significant. That is, one may use metric (26) to monitor the "similarity" between the current traffic behavior and the data set that the optimal CCC design was based on, and redo the optimization when the "similarity" is not satisfactory. This suggests a viable real-time implementation of the design method in changing traffic conditions.

D. Comparison With Receding Horizon Optimal Control

Although the connected cruise control exploits "traffic preview" through motion data of vehicles farther ahead, receding horizon optimal control (RHOC) also exploits "traffic preview" by predicting the motion of the truck's immediate predecessor over a finite time horizon and updating the optimal controller accordingly [13], [14]. Although the energy-optimal CCC design requires much less computational load than an RHOC design, in order to declare the CCC design as an attractive alternative, its real-traffic performance needs to be at least comparable to that of an RHOC design. Therefore, here, we compare the performance of the CCC design presented above to an RHOC design over real traffic data. The details of the RHOC design can be found in [26] which is based on [13], [14].

We remark that the parameters for the RHOC problem are chosen such that the achieved car-following performance is comparable to that of the CCC design. The RHOC problem is discretized with $\Delta T = 0.1$ [s] and the resulting nonlinear programming problem is solved by the open-source interior point solver IPOPT [27]. Due to the nonconvex and nonlinear nature of the problem, the solver cannot guarantee global optimality. It may also encounter infeasibility or fail to converge (exceed a maximum number of iterations). In such cases, the benchmark controller with zero time delay is used, although this rarely happens for the RHOC tests reported in this section.

Previous studies suggest that the length of the preview horizon has a large effect on the performance of the RHOC controllers [15]. Thus, we vary the preview horizon T from 2 [s] to 15 [s] and show the total fuel consumption of RHOC design at the end of the simulation as a brown curve in Fig. 7 for the data set in Fig. 2(a). We also mark the fuel consumption corresponding to the benchmark design (dashed-dotted blue line) and the energy-optimal CCC design (solid green line) in Fig. 7. As it can be seen, RHOC requires a preview horizon to be larger than 9.5 [s] in order to outperform the energy-optimal CCC design. When the preview horizon is shorter than 5.5 [s], the RHOC performs even worse than the benchmark design. Indeed, similar trends are observed for all six data sets, underlining the robustness of these findings.

To take a closer look at the car-following performance, in Fig. 8, we plot the time profiles of headway and speed for the RHOC design with 5 [s] and 10 [s] preview horizons (brown and magenta curves) along with the those for the benchmark design (blue curves) and energy-optimal CCC design (green curves). Note that even for 10 [s] preview horizon, the car-following performance of RHOC is worse than that of the energy-optimal CCC design.

We emphasize that the performance by RHOC design reported above is achieved by assuming perfect knowledge

about the motion of the preceding vehicle. Prediction about preceding vehicle may be available for a few seconds in practice, but most predictions are typically far from perfect (see [28] and [29]). The performance may be improved by careful and extensive tuning of the parameters in the RHOC design, but it would become increasingly more specific for the speed profile and thus less robust. Based on these observations, the data-driven CCC design proposed in this paper can be a desirable alternative to the RHOC method.

V. Conclusion

In this paper, we proposed a data-driven method to optimize energy efficiency and minimize the fuel consumption of a connected automated truck. First, using experimental data of human-driven vehicles in traffic, we demonstrated through high-fidelity simulations that the fuel consumption is significantly influenced by the traffic perturbations. Then, we proposed an analytical, yet data-driven, method to design optimal connected cruise controllers using the Fourier spectra of speed profiles. Evaluating the design on different sets of traffic data we found that utilizing motion information from multiple vehicles ahead not only improved the fuel economy of the connected automated truck, but also enhanced its car-following performance and safety in traffic. Such improvements were also shown to be robust against variations in traffic data. Finally, the proposed data-driven design was shown to be a viable alternative to the RHOC method.

The method proposed in this paper was designed for heavy-duty trucks, but it can potentially be applied to personal vehicles and even to those using alternative power sources. For future research, the proposed method shall be extended to include more information about preceding vehicles and road elevation, and merged with optimization based on geolocation information. The controller shall also be implemented on real heavy-duty trucks and be tested in more diverse traffic scenarios. We remark that safety guarantee may be achieved by selecting the gains properly [30], and a thorough study on safety verification will also be carried out in future research.

References

[1] *Commodity Flow Survey: United States: 2012*, U. S. Dept. Transp., Washington, DC, USA, 2015.

[2] E. Hellström, "Look-ahead control of heavy vehicles," Ph.D. dissertation, Dept. Elect. Eng., Linköping Univ., Linköping, Sweden, 2010.

[3] A. Sciarretta, G. De Nunzio, and L. L. Ojeda, "Optimal ecodriving control: Energy-efficient driving of road vehicles as an optimal control problem," *IEEE Control Syst.*, vol. 35, no. 5, pp. 71–90, Oct. 2015.

[4] C. R. He, H. Maurer, and G. Orosz, "Fuel consumption optimization of heavy-duty vehicles with grade, wind, and traffic information," *J. Comput. Nonlinear Dyn.*, vol. 11, no. 6, pp. 061011-1–061011-12, 2016.

[5] X.-Y. Lu and S. Shladover, "Integrated ACC and CACC development for heavy-duty truck partial automation," in *Proc. Amer. Control Conf.*, May 2017, pp. 4938–4945.

[6] M. Wang, W. Daamen, S. P. Hoogendoorn, and B. van Arem, "Cooperative car-following control: Distributed algorithm and impact on moving jam features," *IEEE Trans. Intell. Transp. Syst.*, vol. 17, no. 5, pp. 1459–1471, May 2016.

[7] K. C. Dey *et al.*, "A review of communication, driver characteristics, and controls aspects of cooperative adaptive cruise control (CACC)," *IEEE Trans. Intell. Transp. Syst.*, vol. 17, no. 2, pp. 491–509, Feb. 2016.

[8] A. Alam, "Fuel-efficient heavy duty vehicle platooning," Ph.D. dissertation, School Elect. Eng., Kungliga Tekniska Hogskolan, Stockholm, Sweden, 2014.

[9] V. Turri, B. Besselink, and K. H. Johansson, "Cooperative look-ahead control for fuel-efficient and safe heavy-duty vehicle platooning," *IEEE Trans. Control Syst. Technol.*, vol. 25, no. 1, pp. 12–28, Jan. 2017.

[10] S. E. Shladover, C. Nowakowski, X.-Y. Lu, and R. Ferlis, "Cooperative adaptive cruise control: Definitions and operating concepts," *Transp. Res. Rec., J. Transp. Res. Board*, vol. 2489, no. 1, pp. 145–152, 2015.

[11] B. Asadi and A. Vahidi, "Predictive cruise control: Utilizing upcoming traffic signal information for improving fuel economy and reducing trip time," *IEEE Trans. Control Syst. Technol.*, vol. 19, no. 3, pp. 707–714, May 2011.

[12] S. Lefèvre, A. Carvalho, and F. Borrelli, "A learning-based framework for velocity control in autonomous driving," *IEEE Trans. Autom. Sci. Eng.*, vol. 13, no. 1, pp. 32–42, Jan. 2016.

[13] J. Jing, E. Özatay, A. Kurt, J. Michelini, D. Filev, and Ü. Özgüner, "Design of a fuel economy oriented vehicle longitudinal speed controller with optimal gear sequence," in *Proc. IEEE Conf. Decis. Control*, Dec. 2016, pp. 1595–1601.

[14] S. E. Li *et al.*, "Performance enhanced predictive control for adaptive cruise control system considering road elevation information," *IEEE Trans. Intell. Vehicles*, vol. 2, no. 3, pp. 150–160, Sep. 2017.

[15] C. R. He and G. Orosz, "Saving fuel using wireless vehicle-to-vehicle communication," in *Proc. Amer. Control Conf.*, May 2017, pp. 4946–4951.

[16] K. K. McDonough, "Developments in stochastic fuel efficient cruise control and constrained control with applications to aircraft," Ph.D. dissertation, Univ. Michigan, Ann Arbor, MI, USA, 2015.

[17] A. Rajeswaran, K. Lowrey, E. V. Todorov, and S. M. Kakade, "Towards generalization and simplicity in continuous control," in *Advances in Neural Information Processing Systems*, I. Guyon *et al.*, Eds. New York, NY, USA: Curran Associates, 2017, pp. 6550–6561.

[18] G. Orosz, "Connected cruise control: Modelling, delay effects, and nonlinear behaviour," *Vehicle Syst. Dyn.*, vol. 54, no. 8, pp. 1147–1176, 2016.

[19] J. I. Ge and G. Orosz, "Connected cruise control among human-driven vehicles: Experiment-based parameter estimation and optimal control design," *Transp. Res. C, Emerg. Technol.*, vol. 95, pp. 445–459, Oct. 2018.

[20] J. I. Ge, S. S. Avedisov, C. R. He, W. B. Qin, M. Sadeghpour, and G. Orosz, "Experimental validation of connected automated vehicle design among human-driven vehicles impacts on traffic safety and effciency," *Trans. Res. C*, vol. 91, pp. 335–352, Jun. 2018.

[21] N. I. Li, C. R. He, and G. Orosz, "Sequential parametric optimization for connected cruise control with application to fuel economy optimization," in *Proc. IEEE 55th Conf. Decis. Control*, Dec. 2016, pp. 227–232.

[22] C. R. He, J. I. Ge, and G. Orosz, "Data-based fuel-economy optimization of connected automated trucks in traffic," in *Proc. Annu. Amer. Control Conf.*, Jun. 2018, pp. 5576–5581.

[23] L. Zhang, J. Sun, and G. Orosz, "Hierarchical design of connected cruise control in the presence of information delays and uncertain vehicle dynamics," *IEEE Trans. Control Syst. Technol.*, vol. 26, no. 1, pp. 139–150, Jan. 2018.

[24] L. Zhang and G. Orosz, "Motif-based design for connected vehicle systems in presence of heterogeneous connectivity structures and time delays," *IEEE Trans. Intell. Transp. Syst.*, vol. 17, no. 6, pp. 1638–1651, Jun. 2016.

[25] J. I. Ge and G. Orosz, "Optimal control of connected vehicle systems with communication delay and driver reaction time," *IEEE Trans. Intell. Transp. Syst.*, vol. 18, no. 8, pp. 2056–2070, Aug. 2017.

[26] (Jan. 2019). *Supplemental Material*. [Online]. Available: http://www-personal.umich.edu/~hchaozhe/TCST2018Sup.pdf

[27] A. Wächter and L. T. Biegler, "On the implementation of an interior-point filter line-search algorithm for large-scale nonlinear programming," *Math. Program.*, vol. 106, no. 1, pp. 25–57, 2006.

[28] J. Jing, D. Filev, A. Kurt, E. Özatay, J. Michelini, and Ü. Özgüner, "Vehicle speed prediction using a cooperative method of fuzzy Markov model and auto-regressive model," in *Proc. IEEE Intell. Vehicles Symp.*, Jun. 2017, pp. 881–886.

[29] C. Sun, X. Hu, S. J. Moura, and F. Sun, "Velocity predictors for predictive energy management in hybrid electric vehicles," *IEEE Trans. Control Syst. Technol.*, vol. 23, no. 3, pp. 1197–1204, May 2015.

[30] C. R. He and G. Orosz, "Safety guaranteed connected cruise control," in *Proc. Int. Conf. Intell. Transp. Syst.*, 2018, pp. 549–554.

Supplementary Materials for "Fuel Efficient Connected Cruise Control for Heavy-duty Trucks in Real Traffic"

Chaozhe R. He, Jin I. Ge, and Gábor Orosz

I. Approximating the energy consumption

In this section we provide the detailed derivation of the cost function

$$J_n(\mathbf{p}_n) = \sum_{j=1}^{m} \omega_j^2 D_j^2(\mathbf{p}_n)\,. \tag{1}$$

Recall the truck's speed response for a certain parameter set $\mathbf{p}_n$

$$\tilde{v}(t) = \sum_{j=1}^{m} D_j(\mathbf{p}_n)\sin\big(\omega_j t + \theta_j(\mathbf{p}_n)\big), \tag{2}$$

we have

$$v(t) = v^* + \tilde{v}(t) = v^* + \sum_{j=1}^{m} D_j \sin(\omega_j t + \theta_j), \tag{3}$$

where $t \in [t_0, t_\mathrm{f}]$, $\omega_j = j\Delta\omega$, $j = 1,\ldots,m$, and $\Delta\omega = 2\pi/(t_\mathrm{f}-t_0)$. Correspondingly, the acceleration of the truck is

$$\dot{v}(t) = \sum_{j=1}^{m} D_j\omega_j \cos(\omega_j t + \theta_j). \tag{4}$$

Note that the nonlinear function $g(x) = \max(x, 0)$ in (6) can be approximated by

$$\hat{g}(x) = \frac{1}{2}\left(x + \frac{x^2}{\sqrt{\varepsilon + x^2}}\right), \tag{5}$$

for small $\varepsilon > 0$.

In order to relate the motion of a truck to the fuel consumption, we define the cumulative energy consumption for the truck per unit mass

$$w(t) = \int_{t_0}^{t} v(\tilde{t})\, g\Big(\dot{v}(\tilde{t}) + f\big(v(\tilde{t})\big)\Big)\,\mathrm{d}\tilde{t}\,, \tag{6}$$

where $t \in [t_0, t_\mathrm{f}]$ and $g(x) = \max(0, x)$. For vehicles with internal combustion engines, fuel consumption typically increases with the energy consumption $w(t)$. However, as $w(t)$ is defined by the vehicle's motion, it can also be used to evaluate the energy consumption of electric or hybrid vehicles due to speed variations using an appropriate g function.

Since the energy consumption due to physical effects $f(v)$ is shown to be small, we may omit $f(v)$ and approximate the total energy consumption (6) by

$$\hat{w} = \int_{t_0}^{t_\mathrm{f}} v\,\hat{g}\big(\dot{v}\big)\,\mathrm{d}t = \frac{1}{2}\int_{t_0}^{t_\mathrm{f}} \frac{v\,\dot{v}^2}{\sqrt{\varepsilon + \dot{v}^2}}\,\mathrm{d}t\,. \tag{7}$$

Note that

$$\dot{v}^2 = \sum_{j,k=1}^{m} D_j D_k \omega_j\omega_k \cos(\omega_j t + \theta_j)\cos(\omega_k t + \theta_k)\,. \tag{8}$$

Thus, for some $M > 0$, we have

$$\varepsilon \le \varepsilon + \dot{v}^2 \le \varepsilon + \sum_{j,k=1}^{m} D_j\omega_j D_k\omega_k \le M\sum_{j=1}^{m} D_j^2\omega_j^2\,, \tag{9}$$

where in the last step we utilized the Cauchy-Schwarz inequality. Thus, we obtain the bounds

$$\frac{\displaystyle\int_{t_0}^{t_\mathrm{f}} v\,\dot{v}^2\mathrm{d}t}{2\sqrt{M\displaystyle\sum_{j=1}^{m} D_j^2\omega_j^2}} \le \hat{w} \le \frac{\displaystyle\int_{t_0}^{t_\mathrm{f}} v\,\dot{v}^2\mathrm{d}t}{2\sqrt{\varepsilon}}\,. \tag{10}$$

On the other hand,

$$\begin{aligned} v^*\dot{v}^2 =& \frac{v^*}{2}\sum_{j=1}^{m} D_j^2\omega_j^2 - \frac{v^*}{2}\sum_{j=1}^{m} D_j^2\omega_j^2\cos(2\omega_j t + 2\theta_j) \\ &+ \frac{v^*}{2}\sum_{j=1}^{m}\sum_{k=1,k\neq j}^{m} D_j D_k\omega_j\omega_k \\ &\times\Big[\cos\big((\omega_j+\omega_k)t + \theta_j + \theta_k\big) \\ &\quad + \cos\big((\omega_j-\omega_k)t + \theta_j - \theta_k\big)\Big], \end{aligned} \tag{11}$$

and

$$\begin{aligned} \tilde{v}\,\dot{v}^2 =& \sum_{j=1}^{m}\sum_{k=1}^{m}\sum_{l=1}^{m} D_j D_k D_l\omega_j\omega_k \\ &\times\cos(\omega_j t + \theta_j)\cos(\omega_k t + \theta_k)\sin(\omega_l t + \theta_l) \\ =& \frac{1}{4}\sum_{j=1}^{m}\sum_{k=1}^{m}\sum_{l=1}^{m} D_j D_k D_l\omega_j\omega_k \\ &\times\Big[\sin\big((\omega_j+\omega_k+\omega_l)t + \theta_j + \theta_k + \theta_l\big) \\ &\quad - \sin\big((\omega_j+\omega_k-\omega_l)t + \theta_j + \theta_k - \theta_l\big) \\ &\quad + \sin\big((\omega_j-\omega_k+\omega_l)t + \theta_j - \theta_k + \theta_l\big) \\ &\quad - \sin\big((\omega_j-\omega_k-\omega_l)t + \theta_j - \theta_k - \theta_l\big)\Big]. \end{aligned} \tag{12}$$

Thus, adding (11) and (12) and evaluating the integrals, we

obtain

$$\int_{t_0}^{t_\mathrm{f}} v\,\dot{v}^2 \mathrm{d}t = \frac{t_\mathrm{f}-t_0}{2} v^* \sum_{j=1}^{m} D_j^2\omega_j^2 + \frac{t_\mathrm{f}-t_0}{4} \sum_{j=1}^{m-1}\sum_{k\le m-j}^{m} D_j D_k D_{j+k}\omega_j\omega_k \sin(\theta_{j+k}-\theta_j-\theta_k) + \frac{t_\mathrm{f}-t_0}{2} \sum_{j=1}^{m-1}\sum_{k>j}^{m} D_j D_k D_{k-j}\omega_j\omega_k \sin(\theta_j+\theta_{k-j}-\theta_k). \tag{13}$$

Here, we assume the speed oscillations are small compared to the steady-state speed, that is, $v^* \gg D_j$ for $j=1,\dots,m$. Then denoting $\overline{D} = \max\{D_j | j=1,\dots,m\}$. Thus, we have

$$\Big|\sum_{j=1}^{m-1}\sum_{k\le m-j}^{m} D_j D_k D_{j+k}\omega_j\omega_k \sin(\theta_{j+k}-\theta_j-\theta_k)\Big| \le \sum_{j=1}^{m-1}\sum_{k\le m-j}^{m} D_j D_k D_{j+k}\omega_j\omega_k < m\overline{D}\sum_{j=1}^{m}\omega_j^2 D_j^2, \tag{14}$$

and

$$\Big|\sum_{j=1}^{m-1}\sum_{k>j}^{m} D_j D_k D_{k-j}\omega_j\omega_k \sin(\theta_j+\theta_{k-j}-\theta_k)\Big| \le \sum_{j=1}^{m-1}\sum_{k>j}^{m} D_j D_k D_{k-j}\omega_j\omega_k < \frac{m\overline{D}}{2}\sum_{j=1}^{m}\omega_j^2 D_j^2, \tag{15}$$

yielding

$$\frac{(v^*-m\overline{D})(t_\mathrm{f}-t_0)}{2}\sum_{j=1}^{m} D_j^2\omega_j^2 \le \int_{t_0}^{t_\mathrm{f}} v\,\dot{v}^2\mathrm{d}t \le \frac{(v^*+m\overline{D})(t_\mathrm{f}-t_0)}{2}\sum_{j=1}^{m} D_j^2\omega_j^2. \tag{16}$$

Finally, the energy consumption (7) can be bounded

$$\underline{C}\sqrt{\sum_{j=1}^{m} D_i^2\omega_j^2} \le \hat{w} \le \overline{C}\sum_{j=1}^{m} D_j^2\omega_j^2 \tag{17}$$

where

$$\underline{C} = \frac{(v^*-m\overline{D})(t_\mathrm{f}-t_0)}{4\sqrt{M}}, \quad \overline{C} = \frac{(v^*+m\overline{D})(t_\mathrm{f}-t_0)}{4\sqrt{\varepsilon}}. \tag{18}$$

Given $v^* > m\overline{D}$, the energy consumption (7) is bounded by class-$\mathcal{K}$ functions of $\sum_{j=1}^{m} D_j^2\omega_j^2$, which can be used for a robust energy-optimal design; see (1).

II. Receding horizon optimal control (RHOC) design

In this Section we provide some details about the receding horizon optimal control (RHOC) approach.

1) Longitudinal model: We model the longitudinal dynamics as

$$\begin{aligned}\dot{s}(t) &= v(t),\\ \dot{v}(t) &= -f\big(v(t)\big) + u(t).\end{aligned} \tag{19}$$

The dissipation $f(v)$ is still given by

$$f(v) = \frac{1}{m_\mathrm{eff}}(\gamma m\mathrm{g} + k_0 v^2), \tag{20}$$

where g is the gravitational constant, γ is the rolling resistance coefficient, and k_0 is the air drag constant. The effective mass $m_\mathrm{eff} = m + I/R^2$ includes the mass of the vehicle m, the moment of inertia I of the rotating elements, and the wheel radius R [1]. Note that here the feedback structure of the controller u is not predetermined. Moreover, the delays are omitted as we assume that a predictor can accurately predict the current state (and even the future states) of the vehicles.

2) Fuel consumption map and input constraints: Fuel consumption rates are typically given as a function of the engine speed ω_e and engine torque T_e, that is, $q(\omega_\mathrm{e}, T_\mathrm{e})$. Given a well defined gear shift logic one may obtain the fuel consumption as a function of the speed v and the control input u, i.e., $q(v,u)$ [2]. Here we utilize the Willans approximation

$$q(v,u) = \begin{cases} p_2 v\,u + p_1 v + p_0, & \text{if} \quad u \ge 0,\\ p_1 v + p_0,, & \text{if} \quad u < 0,\end{cases} \tag{21}$$

to get analytical approximation of the fuel consumption rate [3]. In particular we have p_2=1.8284 [gs^2/m^2], p_1=0.0209 [g/m], $p_0 = -0.1868$ [g/s] for the truck.

The distinction between the two cases in (21) is made since for $u<0$ the engine torque is set to zero and the brakes are applied. To bypass this nonsmoothness, we define the control inputs u_d and u_b such that

$$u = u_\mathrm{d} + u_\mathrm{b}, \tag{22}$$

with the constraints

$$u_\mathrm{d} \ge 0, \quad u_\mathrm{b} \le 0, \quad u_\mathrm{d}u_\mathrm{b} = 0. \tag{23}$$

Indeed, u_d is related to driving torque, while u_b is related to braking torque. Then (21) can be rewritten as

$$q(v,u_\mathrm{d}) = p_2 v\,u_\mathrm{d} + p_1 v + p_0. \tag{24}$$

Due to the torque limitations of the engine and the brakes the control input u also saturates at u_min and u_max. Here we also take into account the power limitation of the engine, i.e., we have

$$u_\mathrm{min} \le u \le \min\left\{u_\mathrm{max}, \frac{P_\mathrm{max}}{m_\mathrm{eff} v}\right\}, \tag{25}$$

which is visualized in Fig. 1(a). Note that while in the connected cruise controller the power limit was not included in the CCC design, it was still enforced by the high-fidelity simulation platform.

Finally, since RHOC algorithms are typically designed and implemented in discrete-time they may lead to "jerky" trajectories. To avoid this issue, we also pose the constraint

$$\Delta\underline{u} \le \dot{u}_\mathrm{d} + \dot{u}_\mathrm{b} \le \Delta\bar{u}. \tag{26}$$

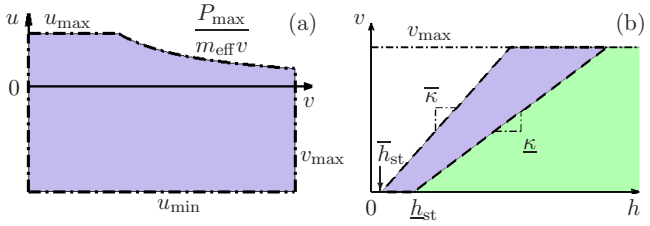


Fig. 1: (a) The working region (25,27) indicated by blue shading in the (v, u)-plane. (b) The constrained region (27,28) indicated by blue shading in (h, v)-plane. The relaxed upper bound (29) extends this by adding the green shading.

3) State Constraints: Corresponding to saturation function (**??**), we set the speed constraint

$$0 \leq v \leq v_{\max}, \tag{27}$$

that is visualized in Fig. 1. Moreover, to generate a car-following behavior similar to that of the CCC controller, we introduce the state constraints

$$\overline{\kappa}\left(h - \overline{h}_{\text{st}}\right) \geq v, \quad \underline{\kappa}\left(h - \underline{h}_{\text{st}}\right) \leq v, \tag{28}$$

using the headway h and the speed v. The parameters are selected so that $\underline{\kappa} \leq \kappa \leq \overline{\kappa}$ and $\underline{h}_{\text{st}} \leq h_{\text{st}} \leq \overline{h}_{\text{st}}$ to make sure that the blue shaded domain shown in Fig. 1(b) includes the curve corresponds to the connected cruise controllers.

It can be shown that with powerful enough propulsion capability, one can have (28) recursively feasible for a finite horizon T. However, with limited power this may not be the case, in particular, when the acceleration capability of the preceding vehicle is larger than that of the truck. To avoid this problem we relax the upper bound in (28) by adding the slack variable η, that is, we set

$$\overline{\kappa}\left(h - \overline{h}_{\text{st}}\right) \geq v, \quad \underline{\kappa}\left(h - \eta - \underline{h}_{\text{st}}\right) \leq v, \tag{29}$$

which extend the shaded domain in Fig. 1(b) with the green part. Note that we do not relax the lower bound as that is safety critical constraint.

4) Implementation: Using the model and constraints listed we set up the following optimal control problem:

$$\min_{u_{\text{d}}, u_{\text{b}}} J = \mu\, \eta^2 + \int_{t_k}^{t_k+T} q(u_{\text{d}}, v)\, \mathrm{d}t, \tag{30}$$

subject to

$$\begin{aligned}
&\begin{bmatrix} \dot{s} \\ \dot{v} \end{bmatrix} = \begin{bmatrix} v \\ -f(v) + u_{\text{d}} + u_{\text{b}} \end{bmatrix}, \\
&u_{\text{d}} \geq 0, \\
&u_{\text{b}} \leq 0, \\
&u_{\min} \leq u_{\text{b}} + u_{\text{d}} \leq \min\left\{u_{\max}, \frac{P_{\max}}{m_{\text{eff}} v}\right\}, \\
&\Delta\underline{u} \leq \dot{u}_{\text{d}} + \dot{u}_{\text{b}} \leq \Delta\bar{u}, \\
&0 \leq v \leq v_{\max}, \\
&\overline{\kappa}\left(h - \overline{h}_{\text{st}}\right) \geq v, \\
&\underline{\kappa}\left(h - \eta - \underline{h}_{\text{st}}\right) \leq v, \\
&\eta \geq 0,
\end{aligned} \tag{31}$$

and we solve this at each $t_k = k\Delta T$, $k = 0, 1, \ldots$. Here μ is the weight on slack variable, $q(u_{\text{d}}, v)$ is given by (24) and $f(v)$ is given by (20). The time horizon T and the sampling period ΔT are chosen such that $T = N\Delta T$ for some $N \in \mathbb{N}$. When solving the optimal control problem the differentials are discretized using explicit Euler method with time step ΔT. Then at each t_k, the first step of the solution is applied over the interval $[t_k, t_k + \Delta T)$ using a zero-order hold, that is,

$$u(t) = u_{\text{d}}(t_k) + u_{\text{b}}(t_k), \quad t \in [t_k, t_k + \Delta T). \tag{32}$$

is commanded in the high-fidelity simulations

We remark that the constraint (26) together with fuel consumption formula (24) implicitly enforces the constraint $u_{\text{d}} u_{\text{b}} = 0$ in (25); see [4]. That is why $u_{\text{d}} u_{\text{b}} = 0$ is not listed in (31) reducing the complexity of the optimal control. Finally, the parameters used in the RHOC are summarized in Table I. Indeed, that the values of $u_{\max}$ and $u_{\min}$ are the same as in the data-based CCC design while we set $\underline{h}_{\text{st}} = h_{\text{st}} = \overline{h}_{\text{st}}$ and $\underline{\kappa} < \kappa < \overline{\kappa}$.

μ	100 [kg/m^2]	ΔT	0.1 [s]
$\overline{h}_{\text{st}}$	5 [m]	$\underline{h}_{\text{st}}$	5 [m]
$u_{\max}$	1 [m/s^2]	$u_{\min}$	-4 [m/s^2]
$\Delta\overline{u}$	4 [m/s^3]	$\Delta\underline{u}$	-4 [m/s^3]
$\underline{\kappa}$	0.4 [1/s]	$\overline{\kappa}$	1 [1/s]

TABLE I: Control parameters for RHOC design.

REFERENCES

[1] C. R. He, H. Maurer, and G. Orosz, "Fuel consumption optimization of heavy-duty vehicles with grade, wind, and traffic information," *Journal of Computational and Nonlinear Dynamics*, vol. 11, no. 6, p. 061011, 2016.

[2] C. R. He, W. B. Qin, N. Ozay, and G. Orosz, "Optimal gear shift schedule design for automated vehicles: Hybrid system based analytical approach," *IEEE Transactions on Control Systems Technology*, vol. 26, pp. 2078–2090, 2018.

[3] L. Guzzella and C. H. Onder, *Introduction to Modelling and Control of Internal Combustion Engine Systems*. Springer, 2004.

[4] C. R. He and G. Orosz, "Saving fuel using wireless vehicle-to-vehicle communication," in *Proceedings of the American Control Conference*, 2017, pp. 4946–4951.